

PACS 07.57.Kp, 73.40.-c

Uncooled $p(\text{Pb}_{1-x}\text{Sn}_x\text{Se})-n(\text{CdSe})$ heterostructure-based photodetector for the far infrared spectral range

Ya.I. Lepikh, I.A. Ivanchenko, L.M. Budienskaya

I.I. Mechnikov Odessa National University,

2, Dvoryanskaya str., 65082 Odessa, Ukraine

Phone/fax: +38(048) 723-34-61, e-mail: ndl_lepikh@onu.edu.ua

Abstract. The possibility to create uncooled photodetector (PD) in the region close to $\lambda = 10 \mu\text{m}$ being based on $p(\text{Pb}_{1-x}\text{Sn}_x\text{Se})-n(\text{CdSe})$ heterojunction has been conceptually and practically confirmed. Design and technology of uncooled thin-film PD based on $p(\text{Pb}_{1-x}\text{Sn}_x\text{Se})-n(\text{CdSe})$ heterojunction in which broad-band CdSe layer is located on the illuminated surface and plays the role of the optical filter with respect to the lower layer of ternary compound. The PD spectral characteristics at room temperature have been researched, which confirms the photoactivity of both heterojunction layers. The mechanism of current flow in the PD structure based on the above heterojunction and the mechanism of the PD samples sensitivity at room temperature in the far infrared spectrum, the determining factor of which is the amount of wide-gap semiconductors where space charge-limited current appears, have been investigated. The uncooled PD detectability typical for polycrystalline structures $10^6 \dots 10^7 \text{ cm}\cdot\text{Hz}^{1/2}/\text{W}$ has been discovered.

Keywords: infrared photodetector, heterostructures, heterojunction, energy band diagram, detectability.

Manuscript received 14.01.14; revised version received 23.07.14; accepted for publication 29.10.14; published online 10.11.14.

1. Introduction

In the far infrared (IR) spectral range ($\lambda > 10 \mu\text{m}$), the highest sensitivity is shown by extrinsic silicon and germanium photodetectors (PD) and also intrinsic PD based on HgCdTe and PbSnTe narrow-gap solid solutions (alloys) cooled to liquid helium and liquid nitrogen temperatures with the detectability $D^* \approx (3 \dots 5) \cdot 10^{10} \text{ cm}\cdot\text{Hz}^{1/2}/\text{W}$ [1]. Since application of cooled photodetectors is complicated and not always desirable, for example, as indicator sensors, the uncooled photodetector creation in this range of the spectrum is quite topical.

Another intrinsic narrow-gap semiconductor is $\text{Pb}_{1-x}\text{Sn}_x\text{Se}$. Electrical properties of $\text{Pb}_{1-x}\text{Sn}_x\text{Se}$ alloy showed the dependence of this phenomenon on the

temperature resistance [2]. Within the temperature range 25 to 180 K, the resistance changes linearly for alloy with $x \approx 0.25$. When temperature exceeds the value 180 K, there takes place a transition from the linear dependence to the nonlinear one, and this temperature is close to the temperature of band inversion T_B . The inversion temperature does not depend on the carrier concentration in the alloy, but changes significantly with the change in alloy composition.

E_g dependence of $\text{Pb}_{1-x}\text{Sn}_x\text{Se}$ alloy on composition and temperature suggested by Strauss [3] has the following form

$$E_g \text{ (eV)} = 0.13 + 4.5 \cdot 10^{-4} T - 0.89x. \quad (1)$$

According to (1), band inversion is observed at the temperatures 77, 195, 300 K and $x = 0.19, 0.25, 0.30$,

Table.

Parameter	Pb _{1-x} Sn _x Se	CdSe
band-gap E_g , eV	0.12	1.67 [6]
electron affinity χ , eV	4.85 (calcul.)	4.95 [6]
work function ϕ , eV	4.97 (experim.)	
lattice type	cubic [6]	hexagonal [7]

respectively. Thus, creation of intrinsic uncooled PD for $\lambda = 10 \mu\text{m}$ is possible. Heterojunction based on Pb_{1-x}Sn_xSe with $x = 0.05$ showed the maximum photosensitivity near $\lambda \sim 10 \mu\text{m}$ at the temperature of liquid nitrogen [4].

The proposed IR photodetecting structure is based on $p(\text{Pb}_{1-x}\text{Sn}_x\text{Se})-n(\text{CdSe})$ thin-film heterojunction.

This heterojunction belongs to the anisotype ones with energy band profiles that can be described within the Anderson model that ignores the states at the boundary [5].

To construct the energy band diagram of $p(\text{Pb}_{1-x}\text{Sn}_x\text{Se})-n(\text{CdSe})$ heterojunction shown in Fig. 1, the constituent semiconductor parameters listed in Table were used. In Fig. 1, the Pb_{1-x}Sn_xSe parameters are denoted by the index 1, and CdSe – by the index 2.

For Pb_{1-x}Sn_xSe ternary compound $E_g = 0.12 \text{ eV}$ was adopted. Pb_{1-x}Sn_xSe electron affinity is obtained by calculation based on the work function $\phi = 4.97 \text{ eV}$ measured using contact potential difference method and the assumptions that the energy of the valence band top E_v is close to the Fermi level energy E_F in narrow-gap semiconductor [5]

$$\chi = \phi - E_g = 4.85 \text{ eV} .$$

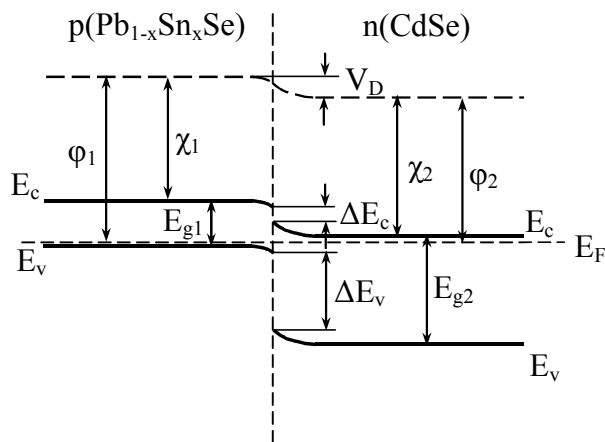


Fig. 1. $p(\text{Pb}_{1-x}\text{Sn}_x\text{Se})-n(\text{CdSe})$ heterojunction energy band diagram.

In accordance with the type system proposed in [5], the expected band diagram of $p(\text{Pb}_{1-x}\text{Sn}_x\text{Se})-n(\text{CdSe})$ heterojunction refers to the type II, in which the narrow-gap semiconductor electron affinity is lower than in the wide-gap ones. An example of the type II heterojunction and an analog of the proposed one with significant difference in the crystal structure is $p(\text{ZnTe})-n(\text{CdSe})$ heterojunction formed also by semiconductors with hexagonal and cubic crystal lattice [6].

According to Table, the energy bands are broken at the boundary of the heterojunction

$$\Delta E_c = \chi_1 - \chi_2 = 0.10 \text{ eV} ,$$

$$\Delta E_v = (\chi_1 + E_{g1}) - (\chi_2 + E_{g2}) = 1.65 \text{ eV} ,$$

and the contact potential difference

$$V_D = \phi_1 - \phi_2 = 0.02 \text{ eV} .$$

In the heterojunction on each side of the interface, the depleted layers that make up the space-charge region were formed. Their thickness is determined using the concentration of majority charge carriers and the barrier height for them. At the layers boundary in this heterojunction type, composed with semiconductors with large E_g , there is a significant difference between the crystal lattice type, the surface states of acceptor type that determines the presence of the barrier in CdSe are formed. Since the barrier height for electrons is much lower than that for holes, and the donor concentration in CdSe is much lower than the acceptor concentration in the layer of narrow-gap Pb_{1-x}Sn_xSe, then a depleted layer is almost entirely located in CdSe. Thus, the determining factor in the mechanism of current flow in the structure is the amount of wide-gap semiconductors, in which the space charge-limited current appears (SCLC).

The absorption of infrared radiation falling onto the heterojunction of the CdSe side is as follows.

The infrared radiation passes through a layer of wide-gap CdSe, which plays the role of the optical window, and excites an electron-hole pairs in the lower layer of narrow-gap Pb_{1-x}Sn_xSe.

The PD construction based on $p(\text{Pb}_{1-x}\text{Sn}_x\text{Se})-n(\text{CdSe})$ heterojunction is shown in Fig. 2. There is CdSe ($E_g = 1.7 \text{ eV}$) wide-gap layer located at the illuminated surface and it serves as the optical narrow-band filter with respect to the lower layer of Pb_{1-x}Sn_xSe ($E_g = 0.12 \text{ eV}$) semiconductor. There are two ohmic contacts attached to both layers. The sample has a square shape formed by the intersection of the narrow- and wide-gap layers with an active area of $10^{-1} \dots 10^{-2} \text{ cm}^2$. The dark resistance of the CdSe high-resistance layer is $10^5 \dots 10^6 \text{ Ohm}$, and that one of Pb_{1-x}Sn_xSe low-resistance layer is $10 \dots 10^3 \text{ Ohm}$. The optimum layers thickness was $1 \dots 3 \mu\text{m}$ for CdSe and $1 \mu\text{m}$ for Pb_{1-x}Sn_xSe.

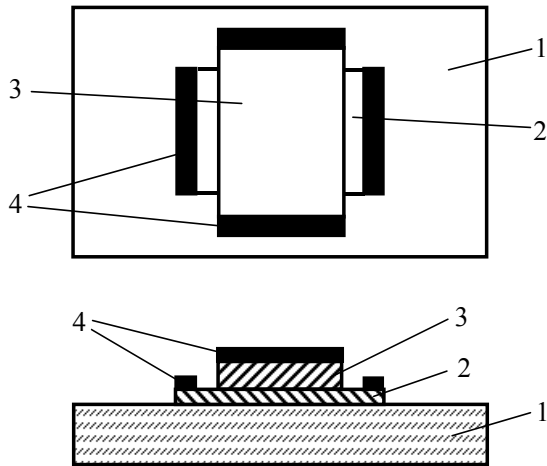


Fig. 2. PD sample construction: 1 – dielectric substrate, 2 – PbSnSe layer, 3 – CdSe layer, 4 – ohmic contacts.

Technological difficulties in manufacturing PD experimental samples are related to the need to obtain film layers of the $Pb_{1-x}Sn_xSe$ solid solution of certain stoichiometric composition, the initial components of which, at relatively close to the melting point are very different in temperature and evaporation rate. $Pb_{1-x}Sn_xSe$ films, obtained by thermal evaporation in vacuum of component compositions from three different sources, and the powder mixture components from one source have shown considerable heterogeneity in composition. The best results are achieved when using evaporation of the $Pb_{1-x}Sn_xSe$ synthesized polycrystalline ingots with subsequent heat treatment of the films [7]. CdSe films production in vacuum flow sheet, similar to most A_2B_6 compounds, is described in [8].

The main proof of the heterojunction and photoactivity operation of both layers are the PD spectral characteristics (Fig. 3) measured across $p(Pb_{1-x}Sn_xSe)-n(CdSe)$ structure and along CdSe top layer. The main peaks near 0.8 and 10.6 μm correspond to intrinsic absorption in CdSe and $Pb_{1-x}Sn_xSe$ layers, respectively. The rise of the sensitivity around 3.0 μm seems to be related with absorption in PbSe binary compound, and around 8.0 μm it is connected with absorption in the ternary $Pb_{1-x}Sn_xSe$ alloy with deviation in the stoichiometric composition.

Investigation of the current flow mechanism in the photodetector structure was carried out using the current-voltage characteristics (CVC) of the samples measured within the temperature range 40...–90°C (Figs 5 and 6).

The presence of ohmic and blocking contacts in the structure of $p(Pb_{1-x}Sn_xSe)-n(CdSe)$ causes the effect of straightening. Straightening the direct and reverse CVC branches shown in double logarithmic coordinates indicates exponential dependence of current on the voltage $I \sim U^n$, where n is the angle of the slope of the

$\lg I(\lg U^n)$ plot. The direct CVC branch (Fig. 5) straightens at room and high temperatures with a slope close to 1, i.e. $I \sim U^2$, and CVC is linear. At lower temperatures, CVC is divided into two sections with different slopes. The initial part (at low voltages) is close to linear, while in the second section $I \sim U^2$. A similar distinction between linear and quadratic parts occurs in the reverse CVC branch in the entire temperature range (Fig. 5). Straightening the $I(U)$ dependence in both branches and the presence of two straightened sections – linear and quadratic – are typical for the SCLC mechanism in the film structure [9].

Measurement of the PD threshold parameters in the far-infrared spectrum was carried out using a CO₂ laser LG-15, emitting at $\lambda = 10.6 \mu m$ with a power up to 35 W. Laser radiation was regulated by the frequency f_m with the mechanical modulator and the power F_l – with the grid attenuator.

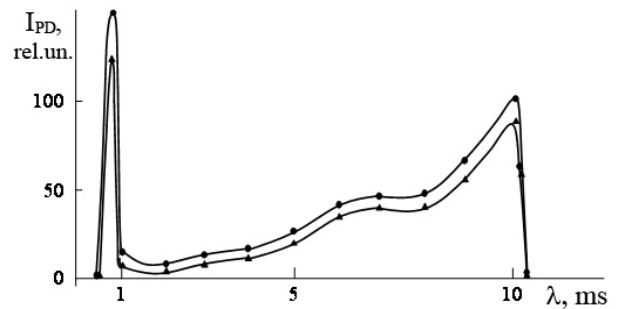


Fig. 3. $p(Pb_{1-x}Sn_xSe)-n(CdSe)$ heterojunction photodetectors spectral characteristics at room temperature: ● – across the structure, ▲ – along CdSe upper layer.

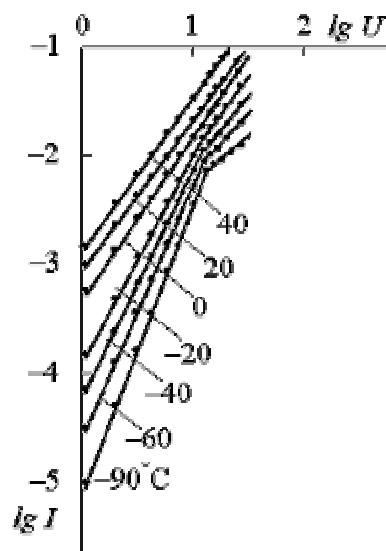


Fig. 4. CVC direct branches at various temperatures.

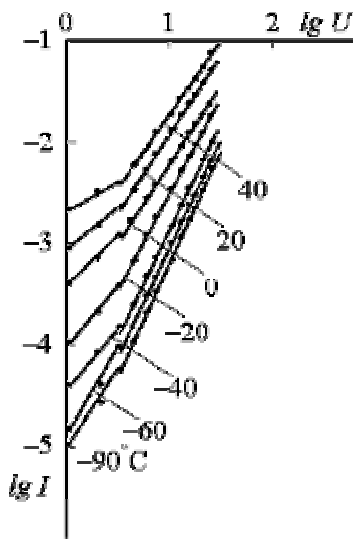


Fig. 5. CVC reverse branches at various temperatures.

Proceeding from the necessity of exposure to the PD entire surface, its area S_{PD} is smaller than cross-sectional area of the laser beam S_l . And the luminous flux F illuminating PD can be expressed as

$$F = \frac{S_{PD}}{S_l} F_l, \quad (2)$$

where F_l is the luminous flux at a certain laser attenuator.

The threshold flux F_p in a single band of an amplifier Δf_a is defined as [10]

$$F_p = \frac{F}{U_s/U_n} \cdot \frac{1}{\sqrt{\Delta f_a}}, \quad (3)$$

where U_s – signal voltage, U_n – voltage noise.

With regard to (2), the working formula to calculate F_p has the form

$$F_p = \frac{S_{PD} F_l}{S_l U_s / U_n} \cdot \frac{1}{\sqrt{\Delta f_a}} \left[\text{W/Hz}^{1/2} \right]. \quad (4)$$

The specific threshold flux F_p referred to PD unit area

$$F_p^* = \frac{F_l \sqrt{S_{PD}}}{S_l U_s / U_n} \cdot \frac{1}{\sqrt{\Delta f_a}} \left[\text{W/cm} \cdot \text{Hz}^{1/2} \right].$$

The specific detectability D^* as a parameter characterizing PD regardless of the sensing element area and of the amplifier channel properties is reverse to F_p

$$D^* = \frac{1}{F_p^*} \left[\text{cm} \cdot \text{Hz}^{1/2} / \text{W} \right]. \quad (5)$$

For the sample series characterized by $S_{PD} = 10^{-1} \dots 10^{-2} \text{ cm}^2$, U_s and $U_n = 10^{-4} \text{ V}$, with $f_m = 50 \text{ Hz}$ and $f_a = 1 \text{ MHz}$, calculated from equations (4) and (5) are values $F_p = 10^{-5} \dots 10^{-7} \text{ W/Hz}^{1/2}$ and, respectively,

$D^* = 10^6 \dots 10^7 \text{ cm} \cdot \text{Hz}^{1/2} / \text{W}$. The obtained values of the threshold parameters are satisfactory for polycrystalline structures.

Conclusions

1. Design of the thin-film uncooled PD based on $p(\text{Pb}_{1-x}\text{Sn}_x\text{Se})-n(\text{CdSe})$ heterojunction has been developed.
2. The spectral characteristics of PD at room temperature containing the main peaks in the CdSe and $\text{Pb}_{1-x}\text{Sn}_x\text{Se}$ areas of intrinsic photoconductivity have been researched.
3. The mechanism of the samples sensitivity in the far infrared spectral region corresponding to the SCLC mechanism has been researched.
4. Photodetector detectability reaches $D^* = 10^6 \dots 10^7 \text{ cm} \cdot \text{Hz}^{1/2} / \text{W}$, which is typical for polycrystalline structures.

References

1. F.F. Sizov, *Photoelectronics for Vision Systems in "Invisible" Spectral Ranges*. Akademiya, Kyiv, 2008 (in Russian).
2. G.F. Hoff, J.R. Dixon // *Solid State Commun.* **10**(5), p. 433-437 (1972).
3. A.J. Strauss // *Phys. Appl.* **157**(3), p. 608-611 (1967).
4. S.P. Chaschin, T.L. Safian, N.S. Baryshev, I.S. Averyanov, N.P. Markina, Photosensitive p-n heterojunctions in $\text{Pb}_{1-x}\text{Sn}_x\text{Se}-\text{PbS}$ system // *Fizika tekhnika poluprovodnikov*, **6**(5), p. 969 (1972), in Russian.
5. B.L. Sharma, R.K. Purokhit, *Semiconductor Heterojunctions*. Sov. Radio, Moscow, 1979 (in Russian).
6. A. Millns, D. Feucht, *Heterojunctions and Metal Semiconductor Junctions*. Mir, Moscow, 1975 (in Russian).
7. N.M. Bondar, V.M. Zheludkov, I.A. Ivanchenko, I.Ya. Shapiro, Uncooled photodetectors for the far infra-red range based on $\text{Pb}_{1-x}\text{Sn}_x\text{Se}$. Abstracts of works of the 1-st Soviet conference on the atmosphere optics, Tomsk, June 23-25, 1986, Part II.
8. Y.F. Waksman, L.M. Budiyanskaya, I.A. Ivanchenko, Colour-detecting photodetector based on thin film heterojunction $p(\text{Cu}_2\text{O})-n(\text{CdS})$ with adjustable spectral sensitivity coordinate // *Photonics*, **12**, p. 76-79 (2003).
9. M.I. Elinson, G.V. Stepanov, P.I. Perlov, V.I. Pokalyakin, *Compilation of Works. Problems of Film Electronics*. Sov. Radio, Moscow, 1966 (in Russian).
10. G.G. Ishanin, E.D. Pankov, A.L. Andreev, G.V. Polschikov, *Radiation Sources and Detectors*. Politekhnik, St.-Petersburg, 1991 (in Russian).